Available online at www.sciencedirect.com
SCIENCE DIRECT®
Polymer 44 (2003) 4229–4238
polymer
www.elsevier.com/locate/polymer

The effect of particle–matrix adhesion on the mechanical behavior of glass filled epoxies: Part 1. A study on yield behavior and cohesive strength

Takafumi Kawaguchi*, Raymond A. Pearson

Materials Science and Engineering, Lehigh University, 5 East Packer Avenue, Bethlehem, PA 18015, USA

Received 3 October 2002; accepted 21 April 2003

Abstract

Basic properties of glass filled epoxy such as yield behavior and cohesive strength, which are important in understanding toughening mechanism, are studied using compression tests and double notch 4 point bending (DN-4PB) tests. Three different glass reinforcements, large glass spheres, small glass spheres, and glass fibers, were treated by different methods and used at different volume fractions ranging from 10 to 30 vol%. The effect of different surface treatments and moisture exposure on the yield behavior is studied. It was found that in all types of formulation the yield stress decreased after moisture exposure and that the yield stress was dependent on the surface treatment both before and after moisture exposure. No treatment and treatment of glass reinforcements with aminopropyltrimethoxysilane coupling agent resulted in relatively higher yield stress. Close observation of microstructure by transmission OM showed that the degree of debonding in the specimens for compression tests was quite dependent on the surface treatment after moisture exposure. The decrease in cohesive strength of the neat specimens were observed after moisture exposure.

Keywords: Epoxy; Yield; Cohesive strength

1. Introduction

Epoxy-based materials have been widely used in engineering components because of their outstanding mechanical, thermal, and electrical properties as well as processability. On the other hand, much effort has been paid to improve the relatively poor fracture resistance of epoxy-based materials. For example, epoxies have been successfully toughened by various means including chemical modification of epoxy molecular structure [1], addition of rubber particles [2,3], addition of thermoplastic phases [4,5], and addition of inorganic fillers [6–21]. Both matrix shear yielding and cohesive strength are important parameters needed for understanding toughening mechanisms [22]. Cohesive strength can be related to the strain energy release rate of a material through a decohesion process occurring at the crack tip. Yield behavior is also related to the strain energy release rate through plastic zone formation at the crack tip [3].

The yield behavior of glass-filled polymers has been studied by several investigators [14,23–25]. Many investigators have shown that the strength of the glass/polymer interface affects the yield stress and that poor adhesion lowers the yield stress [14,24]. The microscopic yield behavior of glass-filled glassy polymers under tensile was extensively investigated by Dekkers and Heikens [23], who showed that microscopic yield behavior was dependent on the strength of glass/polymer interface. A microscopic shear band was observed near the surface of the glass bead at a polar angle of about 45 degree when the bead is adhered to the polycarbonate matrix strongly. Debonding at the interface was observed before microscopic shear band formation when the interface adhesion was poor [23].

Cohesive strength and yield behavior of neat polymers under a triaxial stress state has been studied by several investigators. Such studies utilized bending [26–29] or tensile tests [30] with round-notched specimens or compression tests by flat indenters [31]. Some studies focused

* Corresponding author. Present address: R & D Department, Osaka Gas Co., Ltd, 6-19-9 Torishima, Konohana-ku, Osaka 554-0051, Japan. Tel: +81-6-6462-3441 Fax: +81-6-6462-3436.
E-mail address: tkawa@osakagas.co.jp (T. Kawaguchi).

0032-3861/03/$ - see front matter © 2003 Elsevier Science Ltd. All rights reserved.
doi:10.1016/S0032-3861(03)00371-9

on quantifying the cohesive strength of unfilled polymers. Interestingly, there are few reports in the literature on the cohesive strength measurements of polymer composites in spite of the wealth of information on particle matrix adhesion.

There is an increasing need for the knowledge on the effect of environmental factors such as extreme heat or humidity on mechanical behavior since polymer composites are often applied in situations where the service conditions are more severe. The absorption of moisture usually affects the strength of the matrix–particle interface of the composites as well as the properties of the polymer matrix, In the present study, the basic properties of a glass filled epoxy such as yield behavior and cohesive strength are investigated. Three different glass reinforcements were utilized; large glass spheres (LGS), small glass spheres (SGS), and glass fibers (GF). The surfaces of those reinforcements were treated by different methods and the properties studied as a function of volume fraction of filler. The yield behavior and cohesive strength were studied before and after moisture exposure of the specimens. The results presented in this paper will be extensively used to explain the results of fracture toughness testing [32] and fatigue crack propagation behavior of the same epoxy composites [33,34].

2. Experimental

2.1. Materials

A description of the materials used in this study is shown in Table 1. The epoxy system consisted of diglycidyl ether of bisphenol-A (DGEBA) based epoxy resin (Dow Chemical DER®331, epoxide equivalent weight = 182–192) and bisphenol-A (resin modifier) cured with piperidine. The reaction of epoxy resin with bisphenol-A results in an increased molecular weight between crosslinks [35,36], i.e. chain extension.

Three types of reinforcements were used in this study. Two types were glass spheres (Potters Industry Spheriglass®2900 glass spheres and Spheriglass®10000E). According to the supplier, these glass spheres have a mean diameter of 42 μm and 3.8 μm, respectively. The third type of reinforcement consisted of glass fibers (Owens Corning milled fiber 739DD 1/16″) that have a mean diameter of 15.8 μm and the nominal bulk density of 0.50 g/cm^3.

2.2. Sample preparation

Three different surface treatments were investigated. Some of the reinforcements were treated with 1 wt% solutions (95 wt% methanol and 5 wt% water) of aminopropyltrimethoxysilane (APS) or *n*-butyltrimethoxysilane (*n* BS). Both treatments included a rinse with methanol. The molecular structures of these adhesion promoters are shown in Fig. 1. The adhesion promoters used in this study have either a reactive or non-reactive end group. Amine compounds are known to react with epoxide group and can work as a curing agent for epoxy monomers. It is expected that the amine groups in the APS adhesion promoter will also react with epoxy monomers and form covalent bonds with epoxy matrix, resulting in strong adhesion between the glass reinforcements and the epoxy matrix [37]. For the case of the *n* BS adhesion promoter, the end group is a methyl group. Therefore, only van der Waals type interactions between the adhesion promoter and the epoxy matrix are expected. As a control, the third treatment involved reinforcements with no adhesion promoters on the surfaces and these reinforcements were simply washed with methanol.

The preparation of the epoxy-based matrix involved mixing the epoxy resin and 24 phr bisphenol-A (phr: part per hundred parts resin by weight) at 180 °C under vacuum and subsequently cooling to 80 °C. Then, 10, 20, or 30 vol% of reinforcement was added and mixed under vacuum. Next, 5 phr of piperidine was added and mixed for about 10 min

Table 1
Materials used in this study and their properties

	Materials	Properties	Designation
Matrix resin	Diglycidyl ether of bisphenol-A (DGEBA) DER®331	Epoxide equivalent weight = 182–192	331
Resin modifier	Bisphenol-A	Mp = 153 °C	BisA
Curing agent	Piperidine	Bp = 106 °C	Pip
Reinforcement types			
Large glass spheres	Spheriglass®2900	Mean diameter = 42 μm	LGS
Small glass spheres	Spheriglass®10000E	Mean diameter = 3.8 μm	SGS
Glass fibers	739DD 1.6 mm	Mean diameter = 15.8 μm	GF
		Mean Length = 399 μm	GF
		Nominal density = 0.50 g/cm^3	GF
Surface treatments	Agents	Designation	
Adhesion promoter	Aminopropyltrimethoxysilane	APS	
	n-Butyltrimethoxysilane	*n* BS	
No adhesion promoter	Washed by methanol	NT	

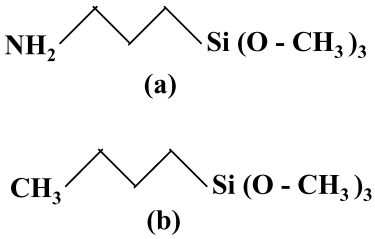

Fig. 1. The molecular structures of the adhesion promoters used in this study. (a) aminopropyltrimethoxysilane; (b) *n*-butyltrimethoxysilane.

under vacuum. The mixture was poured into a mold, that had been preheated at 160 °C. Curing was performed at 160 °C for 6 h. Specimens were cut from the plaques prepared by this procedure. The designation for each material prepared is shown in Table 2.

2.3. Moisture exposure

All test specimens were kept in a humidity chamber set at 85 °C and 85% RH for 1350 h in order to insure equilibrium moisture uptake. Specimens with the size of 6.0 mm × 30.5 mm × 31.8 mm were weighed periodically for the purpose of monitoring moisture uptake.

2.4. Differential scanning calorimetry (DSC)

Materials prepared by the procedure described above were characterized by Differential scanning calorimetry (DSC) using TA instruments DSC2920 at a temperature scanning rate of 10 °C/min. Sample size was nominally 10 mg and sealed aluminum pans were used. For glass transition temperature (T_g), the mid-point values are reported as the T_g.

2.5. Yield stress measurement

Yield stress was measured in compression according to the method described in ASTM D695 [38] using an Instron universal testing machine type 5567. Tetragonal-shaped specimens of 6.0 mm × 6.0 mm × 12 mm were used. The cross-head speed was 1.3 mm/min.

2.6. Double notch 4 point bending (DN-4PB) tests

DN-4PB tests have been utilized to investigate structure of damage zone in polymeric materials. Details for the DN-4PB procedures are in Ref. [39]. In this study, DN-4PB tests were carried out in order to determine the critical hydrostatic pressure of the specimens. The schematic of the DN-4PB test is shown in Fig. 2. The same equipment as the compression tests was utilized with a cross-head speed of 2.54 mm/min, and the notch radii of the specimens were nominally 310 μm. The fracture surfaces of the broken specimens were observed using scanning electron microscopy (SEM). SEM was used to determine the size of plastic zones and the location of decohesion, which are necessary for the calculation of critical hydrostatic pressure.

2.7. SEM observations

Fracture surfaces of DN-4PB tests were observed using a JEOL 6300F or Philips XL-30 SEM with an acceleration voltage of 5 kV. The fracture surface was covered with sputtered Au–Pd before examination.

Table 2
Materials prepared in this study and their designations

Matrix	Reinforcements	Volume% of reinforcements	Surface treatmentsof reinforcements	Designation* [a]
331-BisA-Pip	None	–	–	Neat
	LGS	10	APS	LGS(10)-APS
			n BS	LGS(10)-*n* BS
			NT	LGS(10)-NT
		20	APS	LGS(20)-APS
			n BS	LGS(20)-*n* BS
		30	APS	LGS(30)-APS
			n BS	LGS(30)-*n* BS
	SGS	10	APS	SGS(10)-APS
			n BS	SGS(10)-*n* BS
			NT	SGS(10)-NT
		20	APS	SGS(20)-APS
			n BS	SGS(20)-*n* BS
		30	APS	SGS(30)-APS
			n BS	SGS(30)-*n* BS
	GF	10	APS	GF(10)-APS
			n BS	GF(10)-*n* BS
			NT	GF(10)-NT
		20	APS	GF(20)-APS
			n BS	GF(20)-*n* BS

[a] B and A at the end of each designation shows before moisture treatment and after moisture treatment, respectively.

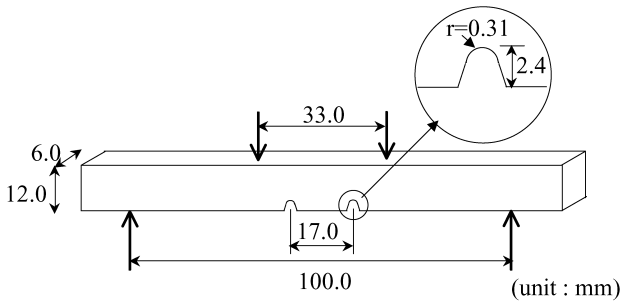

Fig. 2. Schematic of the DN-4PB tests.

2.8. OM observations

The specimens after yield stress tests were polished to the thickness of about 100 μm and were observed with transmission OM (Olympus BH2) under bright field and crossed polars.

3. Results and discussion

3.1. Moisture uptake

Fig. 3 contains the results of weight gain measurements due to moisture uptake for LGS reinforced epoxies exposed to moisture (85% RH) at 85 °C. The weight gain $M(t)$ was calculated using the equation below

$$M(t) = \frac{W - W_0}{W_0} \tag{1}$$

where W_0 and W are the initial weight and the weight at the time t, respectively. The specimens were considered to be saturated with moisture at 1350 h of moisture exposure sine the weight gain data for the most of the resins exhibited a well-defined plateau after 1350 h of moisture exposure. Therefore, humidity exposure was stopped at 1350 h for all of the filled epoxies. The weight gain due to moisture absorption of neat epoxy at saturation was 1.33%. As was expected, formulations with larger volume fraction of reinforcements showed less moisture absorption and slower absorption kinetics as seen in Fig. 3. At the early stages of the weight gain experiments, the absorption curves in Fig. 3 are linear with the square root of time. It is well known that the linear region can be explained using Ficks second law of diffusion [40].

$$\frac{\partial c}{\partial t} = D\frac{\partial^2 c}{\partial x^2} \tag{2}$$

where c is the concentration of the diffusing substance, x is the distance from the surface through the thickness, t is time, and D is the diffusion coefficient. The diffusion coefficient can be calculated from the initial slope of the diffusion curve using Eq. (3) [40,41].

$$D = \pi\left(\frac{sb}{4M_\infty}\right)^2 \tag{3}$$

where s is the slope of the diffusion curve, b is the thickness of the specimen, M_∞ is the moisture content at saturation.

Since specimens prepared in this study have different amount of reinforcements, normalized weight variation $M'(t)$ was defined using the equation below for the purpose of comparing the amount of moisture absorbed by matrix.

$$M'(t) = \frac{M(t)}{1 - V_f} \tag{4}$$

where V_f is the volume fraction of reinforcements in the materials, and $M(t)$ is the measured weight variation. Fig. 4 shows the normalized diffusion coefficient of specimens with LGS calculated from the normalized weight gains. Normalized equilibrium wait gain data can be found in Table 3. Although the specimens with n BS treated LGS showed more moisture absorption at saturation than the ones with APS treated LGS, APS treated LGS had higher moisture diffusion coefficient. Similar trends were observed for SGS and GF. It should be noted that specimens with higher filler loadings had smaller diffusion coefficients. The path of moisture is physically blocked by the higher volume fraction of fillers.

Since the moisture absorption by epoxy has attracted the attention of many investigators, there are numerous reports on this subject [41–46]. However, the differences in the specimen formulation, specimen size, and test conditions make it difficult to compare the data reported by different investigators. Therefore, the diffusion coefficients obtained

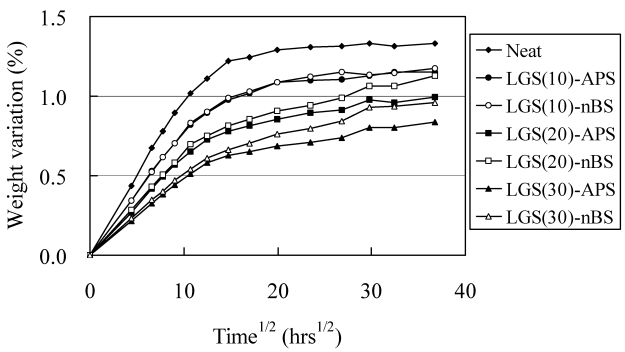

Fig. 3. The results of weight variation measurements for LGS reinforced epoxies during moisture exposure.

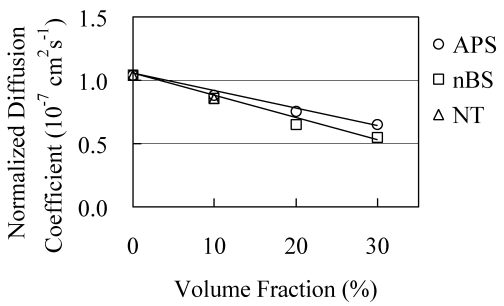

Fig. 4. The normalized diffusion coefficient for LGS reinforced composites calculated from the normalized weight variation.

Table 3
Normalized equilibrium wait gain data for each material

Material	Normalized weight variation at saturation (%)
Neat	1.33
LGS(10)-NT	1.50
LGS(10)-APS	1.28
LGS(20)-APS	1.25
LGS(30)-APS	1.20
LGS(10)-*n* BS	1.31
LGS(20)-*n* BS	1.41
LGS(30)-*n* BS	1.37
SGS(10)-NT	1.39
SGS(10)-APS	1.13
SGS(20)-APS	1.27
SGS(30)-APS	1.21
SGS(10)-*n* BS	1.17
SGS(20)-*n* BS	1.51
SGS(30)-*n* BS	1.56
GF(10)-NT	1.37
GF(10)-APS	1.10
GF(20)-APS	1.09
GF(10)-*n* BS	1.15
GF(20)-*n* BS	1.11

in this study are compared to reported values by choosing studies containing relatively similar formulations. Moreover, for the purpose of comparing our data obtained at 85 °C, it was assumed that Arrhenius relationship shown by Eq. (5) holds for the diffusion coefficients [44].

$$D = D_0 \exp\left(-\frac{E}{RT}\right) \tag{5}$$

where D_0 is constant, E is the activation energy for diffusion, R is the gas constant, and T is the absolute temperature. As is pointed out by other investigators, the diffusion coefficient is dependent on the test temperature and not on the humidity level [44]. Therefore, when comparing diffusion data, it was also assumed that the difference in the humidity level does not affect the diffusion coefficient. As seen in Table 4, our results of $D = 10.4 \times 10^{-8}$ cm^2/s for DGEBA/PIP closely matches the diffusion coefficient of the DGEBA/DICY system reported by De'Néve and Shanahan [42]. There is a discrepancy with the diffusion behavior reported by VanLandingham et al. [44], but this difference may be due to the higher crosslink density and T_g of the DGEBA/PACM system.

3.2. Shift in T_g due to moisture uptake

Fig. 5 shows the results of DSC studies on the neat epoxy before and after moisture exposure. The T_g before moisture exposure was 90 °C, which is consistent with the value reported by other investigators [47,48]. The relatively low T_g indicates that the crosslink density of the epoxy was low. The T_g of the specimen after moisture exposure was 80.2 °C. There was a significant decrease in T_g due to the plasticizing effect of the absorbed moisture. This drop in T_g would also favor faster moisture kinetics at 85 °C.

3.3. Yield stress measurements

Fig. 6(a) and (b) shows the compressive stress–strain curve of the Neat and LGS(10)-APS before (B) and after (A) moisture exposure. As seen in this figure, the specimens after moisture exposure exhibited a decrease in modulus and in yield stresses.

Figs. 7–9 contain the results of yield stress measurements for the formulations containing LGS, SGS, and GF, respectively (before and after moisture exposure). In all cases, the yield stresses increased with increasing volume fraction of reinforcement. Note that the yield strengths before moisture exposure were significantly greater than those after moisture exposure. Also, the yield strengths for specimens containing *n* BS-treated reinforcements were lower than that of specimens with APS-treated reinforcements. There was a considerable change in color of the specimens with *n* BS-treated LGS after the yield point, This color change may be attributable to damage development in the specimens.

Fig. 10 shows the comparison of the results of yield strength measurements in the present report and values reported by Amdouni et al. [14]. The values reported by Amdouni et al. are for composites based on DGEBA epoxy

Table 4
Comparison of diffusion coefficient data obtained by the authors and by other investigators [42,44]

Formulation	Temperature (°C)	RH (%)	D (10^{-8} cm^2 s^{-1})	Ref.
DGEBA/PACM* [a]	25	85	0.3	
	50	85	0.7	[44]
	85	–	2.2* [b]	
DGEBA/DDA* [c]	40	100	0.26	
with Ciba-Geigy Xb3131 fillers	55	100	0.70	[42]
	70	100	3.6	
	85	–	9.9[b]	
DGEBA/bisA/piperidine	85	85	10.4	Present study

[a] bis(para-amino cyclohexyl) methane.
[b] extrapolated by the authors using Arrhenius relationship.
[c] dicyandiamide.

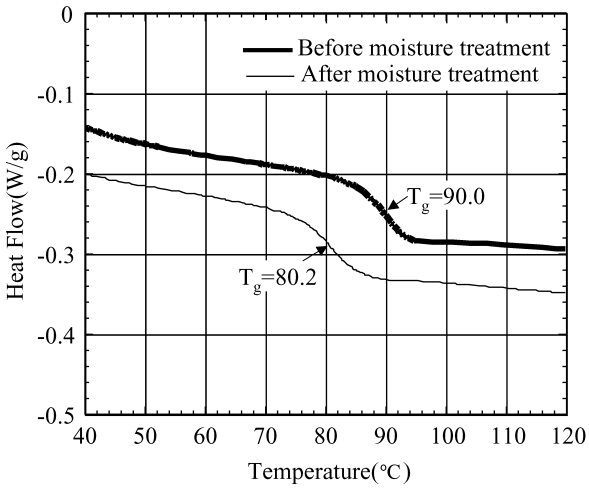

Fig. 5. The results of DCS measurement of the neat epoxy before and after moisture exposure.

cured with benzyldimethylamine reinforced with the glass bead with sizes ranging from 4 to 44 μm that are treated with aminopropyltriethoxysilane. Because of the much higher yield stress of the matrix of their system (108 MPa), normalized yield stresses were calculated by dividing the yield stress (σ_y) by the yield stress of the matrix ($\sigma_{y(matrix)}$). The trend in the dependence of yield stress on the volume fraction was similar as seen in Fig. 10. The

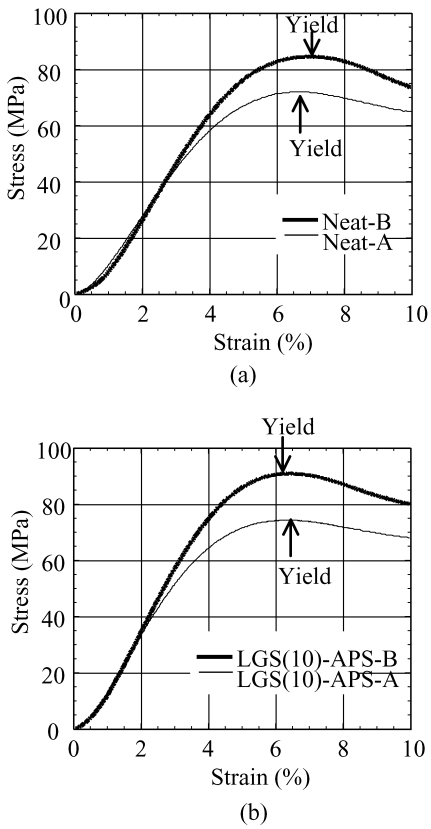

Fig. 6. The stress–strain curve of the Neat and LGS(10)-APS before and after moisture exposure.

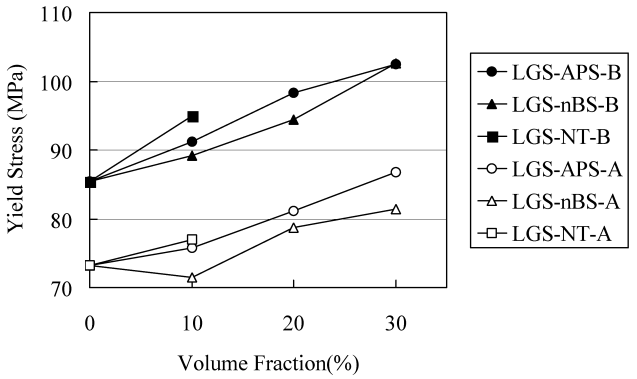

Fig. 7. The results of yield stress measurements for the specimens reinforced with LGS.

discrepancy in the data may be due to the difference in the molecular weight between crosslinks. They reported the T_g of the matrix was about 140 °C, which is much higher than that of the matrix used in this study (90 °C), suggesting that the molecular weight between crosslinks of their system was lower than our system.

3.4. OM observation of specimens after compression tests

Figs. 11–14 show transmission optical microscopy images of LGS reinforced epoxies taken under bright field and crossed polars after compression tests. Figs. 11–14 correspond to LGS(10)-APS-B, LGS(10)-APS-A, LGS(10)-*n* BS-B, and LGS(10)-*n* BS-A, respectively. The direction of compression is shown by arrows in the figures. Before moisture exposure, there was no observable debonding between glass spheres and matrix as seen in Figs. 10(a) and 12(a) in spite of the fact that *n* BS treatment is expected to result in poor adhesion at the matrix–particle interface. This result could be understood from the effect of residual stress around the glass spheres due to the significant difference in coefficient of thermal expansion (CTE) between glass spheres and epoxy matrix. Due to the relatively high CTE of the epoxy matrix, shrinkage of the matrix results in high residual compressive stress around the glass spheres. The residual compressive stress will help the matrix attached to the glass spheres.

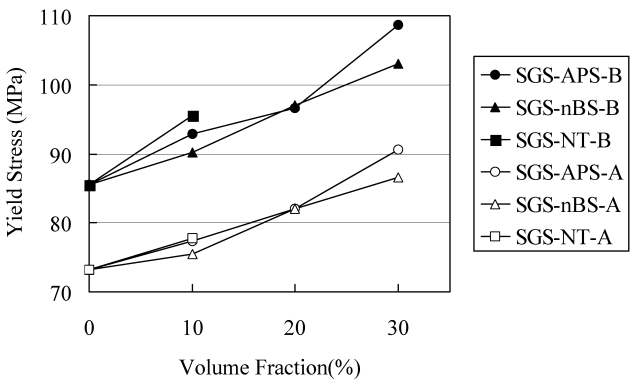

Fig. 8. The results of yield stress measurements for the specimens reinforced with SGS.

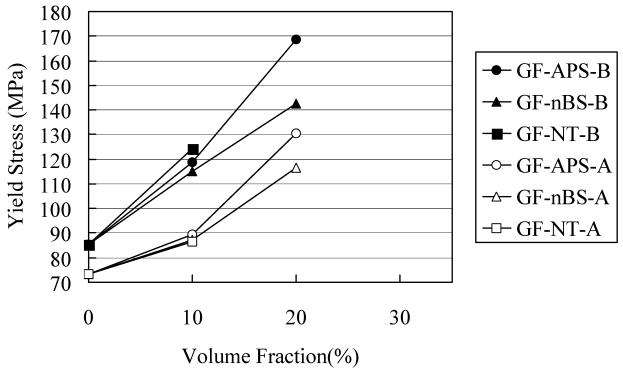

Fig. 9. The results of yield stress measurements for the specimens reinforced with GF.

In Figs. 11(b) and 13(b), the shear bands are clearly observed around the glass spheres under crossed polars. In Figs. 12(b) and 14(b), more diffuse shear bands were observed under crossed polars. Although there have been no model for the sharpness of the shear bands in composites reinforced with hard particles, a model for shear band formation in neat polymers proposed by Bowden may apply [49]. In this model, it was suggested that the sharpness of the shear band is governed by the maximum negative slope in the strain softening part of the stress–strain curve, and that the steeper the slope is, the sharper the shear bands are. In other words, in stress–strain curve, the more rapid stress drop after the yield point results in more sharper shear bands. In fact, the analysis of stress–strain curve obtained in this study showed that the model may be applied to the composites used in this study as seen in Fig. 6(b), which shows the stress–strain curves in the compression tests of LGS(10)-APS-B and LGS(10)-APS-A. Indeed, more rapid stress drop after the yield point can be seen for the neat resin before moisture expose, which explains why the LGS(10)-APS-B system exhibited sharper shear bands.

In the case for LGS(10)-APS-A, as seen in Fig. 12(a), a dimple-like structure around the surface is observed because of partial debonding between the matrix and the glass surface. The partial debonding can be clearly seen by changing the focus point from the outline to somewhat

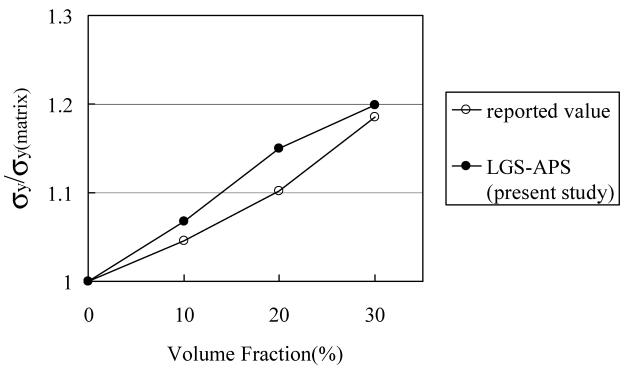

Fig. 10. Comparison of relative yield strength data obtained by the authors and by Amdouni et al.... [14].

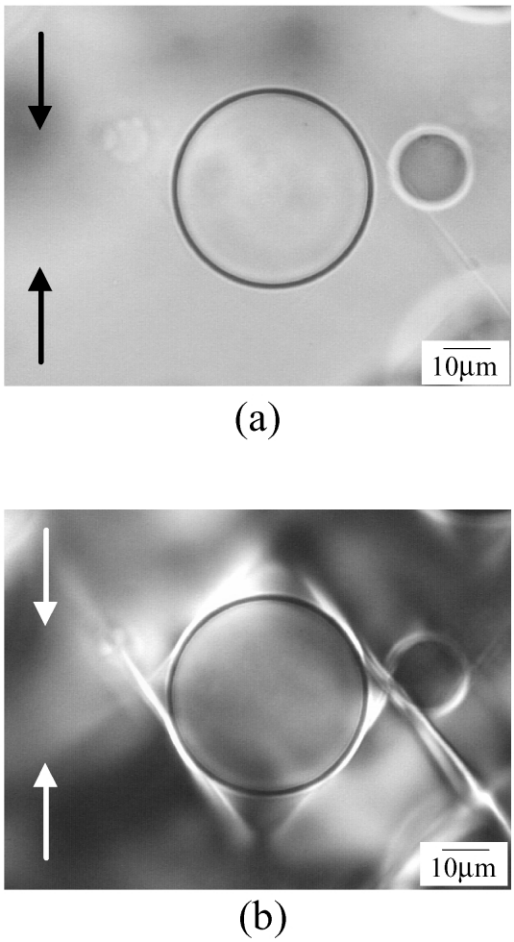

Fig. 11. Transmission OM images of LGS(10)-APS-B after compression test under (a) bright field and (b) crossed polars. The arrows in the figure show the direction of compression.

closer point near the surface (Fig. 12(c)). In the case for LGS(10)-*n* BS-A, as seen in Fig. 14, debonding between matrix and glass spheres around the equator of the sphere is clearly observed which suggest that the matrix–particle adhesion strength decreased significantly after the humidity exposure. The features of the debonded part is similar to that of polycarbonate with poorly adhered spheres [23]. The debonding observed for *n* BS treated glass spheres can be understood from the fact that the interaction between *n* BS coupling agent and matrix is essentially weak and that moisture exposure decreased the residual compressive stress around the glass spheres. Therefore, particle–matrix debonding is the cause of the greater decrease in yield stress of this material as shown in Fig. 7 and for the change in the color described above.

3.5. Determination of critical hydrostatic pressure by DN-4PB tests

The cohesive strength of polymers can be determined by a critical hydrostatic pressure. It is well known that in notched specimens, fracture originates at the boundary of

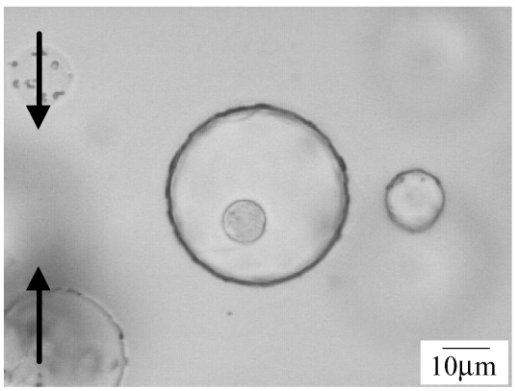

(a)

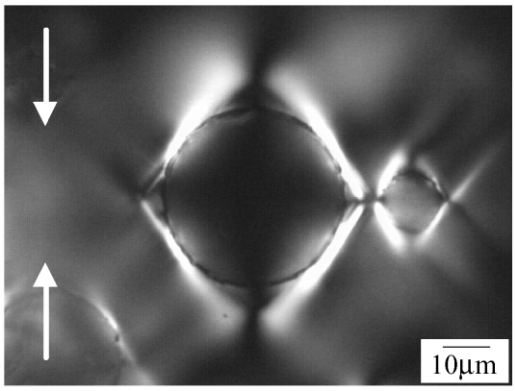

(b)

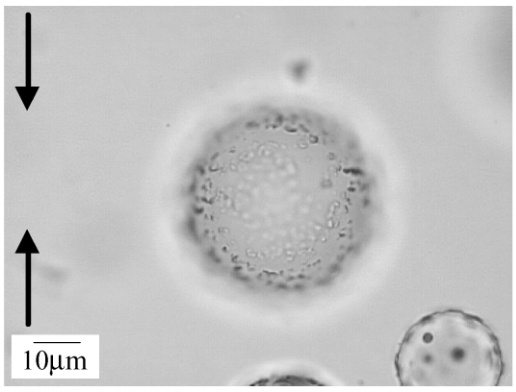

(c)

Fig. 12. Transmission OM images of LGS(10)-APS-A after compression test under (a) bright field, (b) crossed polars, and (c) bright field but focusing on different point. The arrows in the figure show the direction of compression.

plastic and elastic region ahead of the notch. It has been shown that the critical hydrostatic pressure can be calculated from the maximum extent of the plastic region, in other words, the point of crack initiation. Although the equation for the relationship between critical hydrostatic pressure (S_c) and the maximum extent of the plastic zone (r_m) for the materials which exhibit pressure-dependent

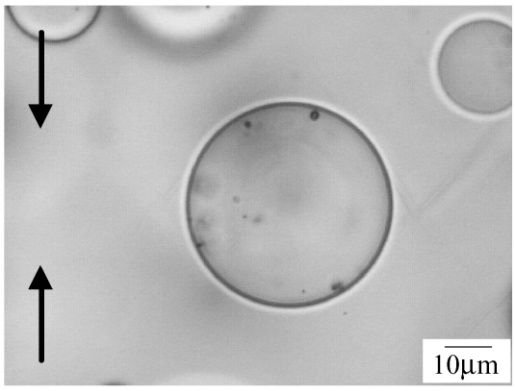

(a)

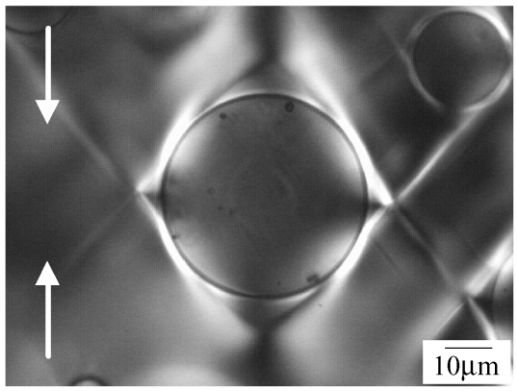

(b)

Fig. 13. Transmission OM images of LGS(10)-*n* BS-B after compression test under (a) bright field and (b) crossed polars. The arrows in the figure show the direction of compression.

yield behavior is reported [30], the equation for pressure-independent materials was used in this study as shown below [29].

$$S_c = \tau\left\{1 + 2\ln\left(\frac{r_m}{\rho}\right)\right\} \tag{6}$$

where ρ is the notch radius, and τ is the shear yield stress. The shear yield stress τ can be calculated by the von Mises yield criterion using the yield stress in uniaxial compression tests as shown below.

$$\tau = \frac{\sigma_y}{\sqrt{3}} \tag{7}$$

Fig. 15 show S_c of neat epoxy before and after moisture exposure. As seen in the figure, the decrease in S_c after moisture exposure was observed. The decrease was due to the absorbed moisture that reduced the strength of molecular interactions between polymer chains.

Attempts were made to determine the S_c values for the composites as well as the neat epoxy. Fig. 16 shows the results of S_c measurements of the epoxy composites reinforced by LGS. As seen in the figure, unexpectedly high S_c values were obtained especially after moisture

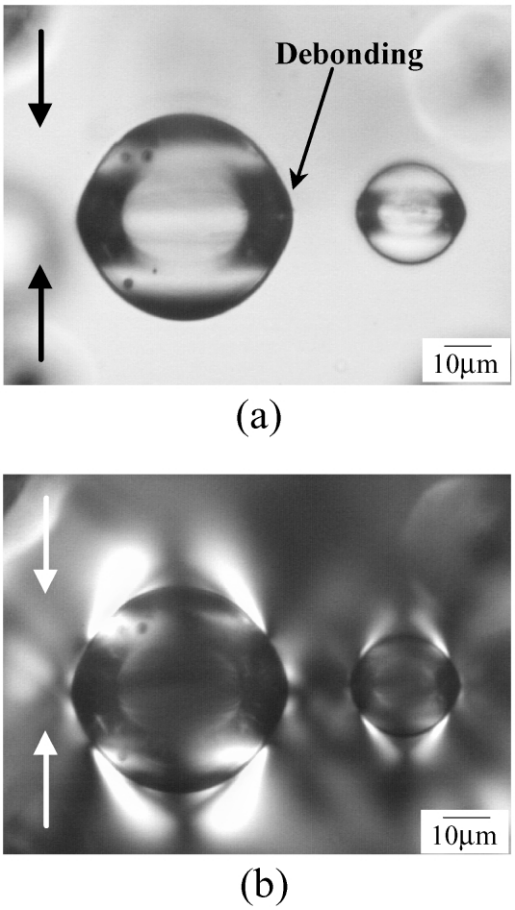

Fig. 14. The transmission OM images of LGS(10)-*n* BS-A after compression test under (a) bright field and (b) crossed polars. The arrows in the figure show the direction of compression.

exposure. Although it is assumed that the material is uniform in the calculation of S_c by Eq. (6), the composites contain non-uniform stress fields due to the presence of the reinforcements. Also, considerable particle–matrix debonding and successive dilatational deformation of matrix was observed for the composites after moisture exposure as shown in Fig. 17, which shows the fracture surface in the plastic region of LGS(10)-*n* BS-A. Debonding at the matrix–particle interface decreased the triaxiality in the matrix leading to an unexpectedly large plastic zone and

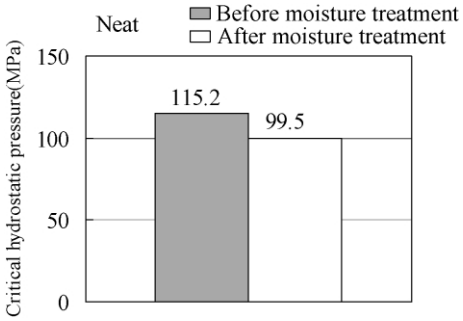

Fig. 15. The calculation results of critical hydrostatic pressure for neat specimens.

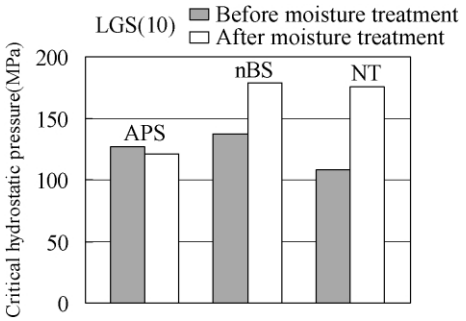

Fig. 16. The calculation results of critical hydrostatic pressure for LGS(10).

high 'apparent S_c'. Similar observation was reported for rubber toughened epoxies by Yee et al. [50]. They performed 4 point bending tests on symmetrical double-edge double-notched specimens of neat and rubber toughened epoxy and reported that the cavitation of rubber particles relieved the triaxial stress state of matrix resulting in relatively large plastic deformation. Therefore, it may be concluded that this methods is not applicable for the cohesive strength measurement of composite materials.

4. Conclusions

The basic properties of glass filled epoxy such as yield behavior and cohesive strength were investigated using three different glass reinforcements; LGS, SGS, and GF. The effect of surface treatment and filler content was examined. Special attention was paid to the effect of different surface treatments and moisture exposure on the yield behavior. It was found that the yield stress decreased after moisture exposure for all of the formulations investigated. Moreover, the yield stress before and after moisture exposure was dependent on the surface treatment. Treating glass spheres with *n* BS resulted in a decrease in yield stress (for both wet and dry conditions). Transmission

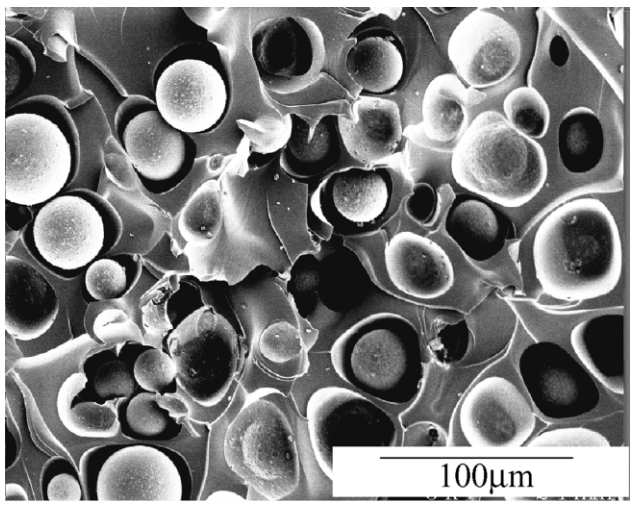

Fig. 17. The SEM image of the fracture surface of the DN-4PB tests for LGS(10)-*n* BS-A.

OM observations revealed that the degree of debonding was quite dependent on the surface treatment after moisture exposure. A study on cohesive strength showed that the cohesive strength of the neat epoxy decreased after moisture exposure. The 'apparent' cohesive strength of composites was unexpectedly high especially after moisture exposure because of the debonding at the matrix–particle interface resulted in enhanced yielding of the matrix. These results showed limited utility for characterizing the cohesive strength of composites.

Acknowledgements

This work was supported by Osaka Gas Co., Ltd.

References

[1] Sue H-J, Puckett PM, Bertram JL, Walker LL. In: Pearson RA, Sue H-J, Yee AF, editors. ACS symposium series 759, toughening of plastics. Washington DC: American Chemical Society; 2000. p. 171.
[2] Kinloch AJ, Shaw SJ, Tod DA, Hunston DL. Polymer 1983;24:1341.
[3] Pearson RA, Yee AF. J Mater Sci 1986;21:2475.
[4] Bucknall CB, Gilbert AH. Polymer 1989;30:213.
[5] Pearson RA, Yee AF. Polymer 1993;34:3658.
[6] Moloney AC, Kausch HH, Stieger HR. J Mater Sci 1983;18:208.
[7] Moloney AC, Kausch HH, Stieger HR. J Mater Sci 1984;19:1125.
[8] Moloney AC, Kausch HH, Kaiser T, Beer HR. J Mater Sci 1987;22:381.
[9] Moloney AC, Cantwell WJ, Kausch HH. Polym Composites 1987;8:314.
[10] Cantwell WJ, Smith JW, Kausch HH, Kaiser T. J Mater Sci 1990;25:633.
[11] Spanoudakis J, Young RJ. J Mater Sci 1984;19:473.
[12] Spanoudakis J, Young RJ. Mater Sci 1984;19:487.
[13] Guild FJ, Young RJ. J Mater Sci 1989;24:298.
[14] Amdouni N, Sautereau H, Gerard JF. J Appl Polym Sci 1992;46:1723.
[15] Nakamura Y, Yamaguchi M, Okubo M, Matsumoto T. Polymer 1992;33:3415.
[16] Azimi HR, Pearson RA, Hertzberg RW. J Appl Polym Sci 1995;58:449.
[17] Lee J, Yee AF. Polymer 2000;41:8363.
[18] Lee J, Yee AF. Polymer 2000;41:8375.
[19] Lee J, Yee AF. Polymer 2001;42:577.
[20] Lee J, Yee AF. Polymer 2001;42:589.
[21] Lee J, Yee AF. J Appl Polym Sci 2001;79:1371.
[22] Thouless MD, Du J, Yee AF. In: Pearson RA, Sue HJ, Yee AF, editors. ACS symposium series 759, toughening of plastics. Washington DC: American Chemical Society; 2000. p. 71.
[23] Dekkers ME, Heikens D. J Mater Sci 1984;19:3271.
[24] Dekkers ME, Heikens D. J Appl Polym Sci 1985;30:2389.
[25] Ishai O, Cohen LJ. J Compos Mater 1968;2:302.
[26] Kitagawa M. J Mater Sci 1982;17:2514.
[27] Kitagawa M, Maruyama H. J Mater Sci 1984;19:1863.
[28] Crawford ED. Proceeding ANTEC 2002, Society of Plastic Engineers, San Francisco, May 2002. p. 3172.
[29] Narisawa I, Maruyama T, Ogawa H. Polymer 1982;23:291.
[30] Narisawa I, Ishikawa M, Ogawa H. J Mater Sci 1980;15:2059.
[31] Kells D, Mills NJ. J Mater Sci 1982;17:1963.
[32] Kawaguchi T, Pearson RA. Polymer 2003: in press.
[33] Kawaguchi T, Pearson RA. submitted to Polymer.
[34] Kawaguchi T, Pearson RA. submitted to Polymer.
[35] Reinking NH, Barnabeo AE, Hale WF. J Appl Polym Sci 1963;7:2135.
[36] Levita G, Marchetti A, Lazzeri A, Frosini V. Polym Compos 1987;8:141.
[37] Arkles B. Chemtech 1977;7:766.
[38] Annual Book of ASTM Standards 2001; vol. 08.01. p. 76.
[39] Sue H-J, Yee AF. J Mater Sci 1993;28:2975.
[40] Shen CH, Springer GS. J Compos Mater 1976;10:2.
[41] Maggana C, Pissis P. J Appl Polym Sci B: Polym Phys 1999;37:1165.
[42] De'Néve B, Shanahan MER. Polymer 1993;34:5099.
[43] MZanni-Deffarges MP, Shanaham MER. Int J Adhes Adhes 1995;15:137.
[44] VanLandingham MR, Eduljee RF, Gillespie JWJ. J Appl Polym Sci 1999;71:787.
[45] Ivanova KI, Pethrick RA, Affrossman S. J Appl Polym Sci 2001;82:3468.
[46] Uschitsky M, Suhir E. J Electron Packaging 2001;123:47.
[47] Levita G. Am Chem Soc Advan Chem Ser 1989;222:93.
[48] Yee AF, Pearson RA. J Mater Sci 1986;21:2462.
[49] Bowden PB. Philos Mag 1970;22:455.
[50] Yee AF, Li D, Li X. J Mater Sci 1993;28:6392.